

Robust Blind Deconvolution with Convolution-Spectrum-Based Kernel Regulariser and Poisson-Noise Data Terms

Martin Welk

Institute of Biomedical Image Analysis,
Private University for Health Sciences, Medical Informatics and Technology (UMIT),
Eduard-Wallnöfer-Zentrum 1, 6060 Hall/Tyrol, Austria
martin.welk@umit.at

Abstract. In recent work by Liu, Chang and Ma a variational blind deconvolution approach with alternative estimation of image and point-spread function was presented in which an innovative regulariser for the point-spread function was constructed using the convolution spectrum of the blurred image. Further work by Moser and Welk introduced robust data fidelity terms to this approach but did so at the cost of introducing a mismatch between the data fidelity terms used in image and point-spread function estimation. We propose an improved version of this robust model that avoids the mentioned inconsistency. We extend the model to multi-channel images and show experiments on synthetic and real-world images to compare the robust variants with the method by Liu, Chang and Ma.

1 Introduction

Since noise and blur are the two most important and ubiquitous sources of degradations in virtually all modalities of image acquisition, methods to enhance images degraded by blur have been an object of intensive research since the early times of image processing. Blur is a spatial redistribution of image intensities; in the simple case when the redistribution follows the same spatial pattern at all image locations it is modelled by convolution of the (unobservable) sharp image g with a space-invariant *point-spread function (PSF)* h as convolution kernel, i.e.

$$f = g * h + n, \quad (1)$$

where f denotes the observed degraded image, and additive noise n has been included in the model. In a similar way spatially variant blur can be modelled by replacing the convolution $*$ in (1) with a Fredholm integral operator. Methods that aim at a computational (approximate) inversion of the blur process (1) (or its more general space-invariant version that we will not treat any further here) are called *deconvolution*. Two types of deconvolution problems are to be distinguished: Non-blind deconvolution assumes that the image f as well as the PSF h are known, and an image u is to be found that fulfils $f \approx u * h$, such that u can be considered as an approximation of g . Blind deconvolution methods take only an image f as input and aim at reconstructing u and h

at the same time. Both types of deconvolution problems are ill-posed inverse problems but of course blind deconvolution is the harder of the two.

One class of approaches to blind deconvolution are variational models that involve minimisation of an energy functional of type [2, 20]

$$E(u, h) = F(f, u * h) + \alpha R_u(u) + \beta R_h(h) \quad (2)$$

where $F(f, u * h)$ is a data fidelity term that penalises deviations from the blur equation $f = u * h$, and brings in the information of the observed image; possible choices will be discussed in more detail later in this paper. R_u and R_h are regularisers for the image and PSF, respectively, that encode assumptions on plausible images and PSFs.

Minimisation of (2) is often done by alternating minimisation, which iteratively improves estimates for u and h by minimising, respectively, the reduced functionals

$$E(u) = F(f, u * h) + \alpha R_u(u) , \quad (3)$$

$$E(h) = F(f, u * h) + \beta R_h(h) . \quad (4)$$

Note that (3) alone is just a variational model for non-blind deconvolution.

Regarding images, smoothness requirements play an important role; these can be encoded by regularisers R_u that impose increasing functions of $|\nabla u|$ at each image location as penalisers.

Whereas the suitability of this class of image regularisers is widely agreed in the field, regularisers R_h for PSFs are more difficult to formulate. Transferring the smoothness-based image regularisers to PSFs has been tried early [2, 20], its success has been limited: firstly, smoothness is an adequate characterisation only of some practically relevant PSFs (such as Gaussian blur); secondly, it misses other important properties of PSFs such as locality and sparsity of support. In recent years, maximum a posteriori [?] and machine-learning approaches [13] for the regularisation of h have been proposed.

In [8] a PSF regulariser based on spectra of convolution operators was introduced, and used within an alternating optimisation approach based on an energy functional of type (2). This is an interesting new approach to the estimation of blur as it uses information from the observed image f to constrain the PSF. The data fidelity term in [8] uses classical quadratic penalisation. As it is known from the image processing literature that data fidelity terms based on less-than-quadratic penalisation allow a more robust minimisation, i.e. reduce sensitivity to extreme noise, outliers, and model violations [1, 4, 18, 21], the authors of [9] proposed a modification of the model from [8] with these so-called robust data fidelity terms. This model, however, suffers from a mismatch between the data fidelity terms used in the image and PSF estimation.

Our contribution. In this paper we improve the blind deconvolution model from [9] by using consistently one type of robust data fidelity term in both components of the alternating minimisation model. To this end, we modify the PSF estimation step of [9] to adopt the data fidelity term from [16] that was used in [9] only for image estimation.

To enable the processing of colour images, we state shortly multi-channel versions of the blind deconvolution model from [9] as well as of the new model. We present experiments on synthetic test images without and with noise that show the viability of the new model and illustrate the usefulness of the robust blind deconvolution models for noisy input data, and on a real-world colour image.

Structure of the paper. The two components of alternating minimisation models as they are used in [8, 9] and our new model are discussed in the next two sections: Section 2 recalls the image estimation models from [6, 14, 16] that are used in [8, 9] and also in the present paper. Section 3 is devoted to PSF estimation; it recalls the PSF regularisation procedures from [8, 9], and introduces our further modification of the latter model. Section 4 translates the estimation procedures to multi-channel images. Section 5 presents experimental results. Section 6 concludes the paper with a short summary and outlook.

2 Image Estimation

The estimation of the image u in the alternating minimisation of (2) is a non-blind deconvolution based on minimising (3) for which several methods exist in the literature. We recall shortly the approaches chosen in [8] and [9] for this purpose.

Krishnan-Fergus method [6]. In [8] the method from [6] is used for the non-blind deconvolution step. Like the very similar method published earlier in [14], it aims at minimising a functional (3) in which the quadratic data fidelity term

$$F(f, u * h) = \int_{\Omega} \varrho(f, u * h) \, d\mathbf{x} , \quad (5)$$

$$\varrho(f, v) \equiv \varrho_{\text{quad}}(f, v) := (f - v)^2 , \quad (6)$$

is combined with a regulariser R_u of type

$$R_u(u) = \int_{\Omega} |\nabla u|^\nu \, d\mathbf{x} =: \int_{\Omega} \Psi(|\nabla u|^2) \, d\mathbf{x} , \quad (7)$$

where ν equals 1 in [14], and can take different discrete values in [6]; in [8] the case $\nu = 1$ is used, i.e. R_u is a total variation (TV) regulariser [12]. In [6, 14] the functional $E(u)$ is rewritten using auxiliary quantities w_x, w_y into a so-called half-quadratic functional, which is then minimised by an iterative procedure that alternates between updating w_x, w_y by (nonlinear) shrinkage applied to the gradient components u_x, u_y , and updating u by a linear filter step via the Fourier domain.

Robust regularised Richardson-Lucy deconvolution [16]. In [9] the authors pursued the goal to introduce a robust data fidelity term $F(f, u * h)$ into the framework of [8]. In the image estimation step they decided to use the so-called robust regularised Richardson-Lucy deconvolution (RRRL) from [16] which has proven useful in several applications of non-blind deconvolution [3, 11, 17].

RRRL is a fixed-point iteration for a functional (3) with the robust data fidelity term

$$F(f, u * h) = \int_{\Omega} \Phi(\varrho(f, u * h)) \, d\mathbf{x} , \quad (8)$$

$$\varrho(f, v) \equiv \varrho_{\text{RL}}(f, v) := v - f - f \ln \frac{f}{v} . \quad (9)$$

Note that unlike ϱ_{quad} from (6) that is related to Gaussian, Laplacean and similar symmetric additive noise types, the residual error measure ϱ_{RL} used here is related to Poisson noise and related types of noise. In (8) it is the argument to a penaliser function $\Phi : \mathbb{R}_0^+ \rightarrow \mathbb{R}_0^+$ that is assumed to increase less than linear; [16] suggests $\Phi(z) = \sqrt{z}$ or, with a numerical regularisation, $\Phi(z) = \sqrt[4]{z^2 + \varepsilon}$. For the regulariser R_u for RRRL different choices are possible, see [16], including the TV regulariser (7) with $\nu = 1$, or regularisers associated with Perona-Malik's isotropic nonlinear diffusion [10]. In [9] the TV regulariser is used, and we will follow this choice in the present paper.

3 Point-Spread Function Estimation

In this section we describe the estimation step for the PSF h in the alternating minimisation scheme. This involves, first, the specification of the PSF regulariser according to [8], and second, its minimisation in combination with a suitable data fidelity term.

For this section, we switch to a discrete setting because the formulation of the spectral decomposition in [8] is done in the finite-dimensional matrix-algebraic setting. We rewrite (4) in the discretised form

$$E(\mathbf{h}) := F(\mathbf{f}, \mathbf{u} * \mathbf{h}) + \beta R_h(\mathbf{h}) \quad (10)$$

with discrete images $\mathbf{f} = (f_{i,j})_{i,j}$, $\mathbf{u} = (u_{i,j})_{i,j}$ and a discrete PSF $\mathbf{h} = (h_{i,j})_{i,j}$. The PSF regulariser R_h and data fidelity term F will be specified in the following subsections.

3.1 Regulariser Based on Convolution Spectrum

Let us now recall the PSF regularisation approach from [8] which also underlies the work in [9] and which will also be adopted in the present paper.

To this end, we start by noticing that, for any given image \mathbf{v} , the convolution $\mathbf{v} * \mathbf{h}$ defines a linear operator on point-spread functions \mathbf{h} . For discrete \mathbf{h} with a support of size $m_x \times m_y$, it is suggested in [8] to embed it into a larger area sized $s_x \times s_y$ with $(s_x, s_y) \approx 1.5(m_x, m_y)$; assuming $n_x \times n_y$ as size of the image \mathbf{v} and adopting the discrete convolution with zero-padding, we have the convolution operator $\mathbf{C}^{\mathbf{v}} : \mathbb{R}^{s_x \times s_y} \rightarrow \mathbb{R}^{(s_x+n_x-1) \times (s_y+n_y-1)}$, $\mathbf{h} \mapsto \mathbf{v} * \mathbf{h}$. Its singular value decomposition yields $s_x s_y$ singular values $\sigma_k(\mathbf{v})$ whose right singular vectors can be identified with singular discrete kernels $\mathbf{h}_k(\mathbf{v})$. Following the terminology of [8], one calls $\sigma_k(\mathbf{v})$ and $\mathbf{h}_k(\mathbf{v})$ the *convolution eigenvalues* and *convolution eigenvectors* of \mathbf{v} .

The core observation of [8], underpinned by theoretical analysis in that source, is that convolution eigenvalues of blurred images $\mathbf{v} = \mathbf{u} * \mathbf{h}$ tend to be substantially smaller than those of the underlying sharp images $\mathbf{v} = \mathbf{u}$. In particular, the convolution eigenvectors belonging to the few smallest convolution eigenvalues $\sigma_k(\mathbf{u} * \mathbf{h})$ are approximately orthogonal to \mathbf{h} under the inner product given by convolution. In other words, $\|\mathbf{h}_k(\mathbf{u} * \mathbf{h}) * \mathbf{h}\| \approx 0$ holds for those k for which $\sigma_k(\mathbf{u} * \mathbf{h}) \approx 0$.

Since the convolution spectrum needs only to be computed for the blurred image, a hard regularisation approach to estimate the convolution kernel \mathbf{h} behind the blurred image $\mathbf{f} = \mathbf{g} * \mathbf{h}$ could use orthogonality of \mathbf{h} with a suitable set of convolution eigenvectors for \mathbf{f} directly. However, this would require a rule (such as a threshold on $\sigma_k(\mathbf{f})$) to

determine the number of convolution eigenvectors to be used. This difficulty is avoided in [8] by using instead a soft constraint with the penaliser $\sum_{k=1}^{s_x s_y} \|\mathbf{h}_k(\mathbf{f}) * \mathbf{h}\|^2 / \sigma_k(\mathbf{f})^2$; the weighting by inverse squared convolution eigenvalues makes the convolution eigenvectors for small convolution eigenvalues dominant in the penalisation without the need for a threshold parameter.

As a refinement to this procedure, the image \mathbf{f} can be preprocessed by a suitable linear filter operator L . Whereas the general principle of convolution orthogonality remains valid due to the commutativity between L and the linear convolution operator, such a modification allows to re-weight the influence of different regions of the image \mathbf{f} on the estimation of \mathbf{h} . Following [8], we choose L as a Laplacean-of-Gaussian (LoG); this correlates with the established fact that the information in near-edge regions of a blurred image is of particular value in blur estimation, compare [19] and other works on blur estimation that exploit this property. The resulting regulariser then reads as [8]

$$R_h(\mathbf{h}) = \sum_{k=1}^{s_x s_y} \frac{\|\mathbf{h}_k(L(\mathbf{f})) * \mathbf{h}\|^2}{\sigma_k(L(\mathbf{f}))^2} \quad (11)$$

with the LoG operator L . Note that \mathbf{h} enters (11) with dimensions $s_x \times s_y$; the actual minimisation, however, will be constrained to \mathbf{h} supported on an $m_x \times m_y$ patch.

Minimisation of the regulariser R_h alone could be used to estimate \mathbf{h} for subsequent non-blind deconvolution, but in this case no regularisation on \mathbf{u} enters the estimation of \mathbf{h} . Indeed, [8] states that such an approach tends to result in over-sharpened images with visible artifacts. One should therefore embed R_h into a joint functional such as (2) with alternating minimisation for \mathbf{u} and \mathbf{h} . To this end, $R_h(\mathbf{h})$ is rewritten as a quadratic form acting on kernels $\mathbf{h} = (h_{i,j})_{i,j}$ of size $m_x \times m_y$, $R_h(\mathbf{h}) = \sum_{i,j,i',j'} H_{i,j;i',j'} h_{i,j} h_{i',j'}$ where the coefficient matrix $\mathbf{H} = (H_{i,j;i',j'})_{i,j;i',j'}$ is the Hessian

$$\mathbf{H} = \sum_{k=1}^{s_x s_y} \frac{\mathbf{C}_{m_x, m_y}^{\mathbf{h}_k(L(\mathbf{f}))} \mathbf{C}_{m_x, m_y}^{\mathbf{h}_k(L(\mathbf{f}))\top}}{\sigma_k(L(\mathbf{f}))^2} \quad (12)$$

which can be pre-computed once for all iterations.

3.2 Robust Data Term in PSF Estimation

In [8] the regulariser (11) written with the Hessian (12) is combined with a quadratic data fidelity term to give a quadratic minimisation problem for \mathbf{h} . In discrete form, the quadratic data fidelity term (compare (5), (6)) reads

$$F(\mathbf{f}, \mathbf{u} * \mathbf{h}) = \sum_{i,j} \varrho(f_{i,j}, v_{i,j}) \quad (13)$$

where $\varrho \equiv \varrho_{\text{quad}}$ is given by (6), and $v_{i,j}$ by

$$\mathbf{v} = (v_{i,j})_{i,j} := \mathbf{u} * \mathbf{h}. \quad (14)$$

The minimality condition of the discrete functional $E(\mathbf{h}) = F(\mathbf{f}, \mathbf{u} * \mathbf{h}) + \beta R_h(\mathbf{h})$ composed of (13) and (11) with (12) is a linear equation system for the entries of \mathbf{h} ,

$$\sum_{i,j} (S_{p,q;i,j} + \beta H_{p,q;i,j}) h_{i,j} = T_{p,q}, \quad \text{for all pixels } (p,q), \text{ with} \quad (15)$$

$$S_{p,q;i,j} = \sum_{r,s} u_{r-i,s-j} u_{r-p,s-q}, \quad T_{p,q} = \sum_{r,s} f_{r,s} u_{r-p,s-q}. \quad (16)$$

This system, which is densely populated, due to R_h , can be solved by standard methods. Since (15) has a high condition number in some cases, regularisation by adding a multiple of the unit matrix to its coefficient matrix may be used for stabilisation.

Robust data term from [9]. In [9] the quadratic data fidelity term F in the PSF estimation step was replaced with a robust data fidelity term [1, 21]

$$F(\mathbf{f}, \mathbf{u} * \mathbf{h}) = \sum_{i,j} \Phi(\varrho(f_{i,j}, v_{i,j})) \quad (17)$$

where $v_{i,j}$ and $\varrho \equiv \varrho_{\text{quad}}$ are given by (14), (6), and $\Phi(z)$ is a penaliser function growing less than z . The L^1 penaliser $\Phi(z^2) = 2|z|$ (or its regularised version $\Phi(z^2) = 2\sqrt{z^2 + \varepsilon}$) is a standard choice here. The minimality condition for the so obtained non-quadratic minimisation problem is a non-linear equation system. Abbreviating

$$\varphi_{r,s} := \Phi'(f_{i,j}, v_{i,j}), \quad (18)$$

the minimality condition system can again be written in the form (15) but

$$S_{p,q;i,j} = \sum_{r,s} \varphi_{r,s} u_{r-i,s-j} u_{r-p,s-q}, \quad T_{p,q} = \sum_{r,s} \varphi_{r,s} f_{r,s} u_{r-p,s-q} \quad (19)$$

now depend on $h_{i,j}$ via $\varphi_{r,s}$. Using this representation, [9] solved the system by iterative linearisation: Given some initial \mathbf{h}^0 , one computes for $l = 0, 1, \dots$ the coefficients $S_{p,q;i,j}$ and $T_{p,q}$ from \mathbf{h}^l and then solves (15) with fixed coefficients to obtain \mathbf{h}^{l+1} . After solving the nonlinear equation system, a sparsification step is used to eliminate negative as well as small positive PSF entries; following [9], values below 0.1 times the 95 %-quantile of PSF entries are set to zero.

The practical viability of this approach has been documented in [9] where experiments showed slight improvements over the method from [8]. However, from a theoretical viewpoint the combination of the L^1 fidelity term based on (6) in the PSF estimation with the one based on (9) in the image estimation breaks the unified model (2) and can only be considered as pragmatic approximation of a proper alternating minimisation of a joint energy functional, which is also righteously pointed out in the conclusion of [9].

Asymmetric robust data term. To address this inconsistency in the method of [9], we combine the regulariser (11) with the a discretised version of the data fidelity term (8), (9), i.e. (17) with $\varrho \equiv \varrho_{\text{RL}}$ as given by (9). As penaliser function Φ we will use in experiments $\Phi(z) = \sqrt{z}$ or an approximation thereof.

From (17), (9), (14) we compute

$$\begin{aligned}
\frac{\partial}{\partial h_{p,q}} F &= 2 \sum_{i,j} \Phi'(\varrho(f_{i,j}, v_{i,j})) \frac{\partial \varrho(f_{i,j}, v_{i,j})}{\partial v_{i,j}} \frac{\partial v_{i,j}}{\partial h_{p,q}} \\
&= 2 \sum_{i,j} \Phi'(\varrho(f_{i,j}, v_{i,j})) \left(1 - \frac{f_{i,j}}{v_{i,j}}\right) u_{i-p,j-q} \\
&= - \sum_{i,j} \frac{2 \Phi'(\varrho(f_{i,j}, v_{i,j}))}{v_{i,j}} (f_{i,j} - v_{i,j}) u_{i-p,j-q}. \tag{20}
\end{aligned}$$

For the joint functional $E(\mathbf{h}) = F + \beta R_h$, we obtain therefore the minimality conditions as a nonlinear equation system in the same form (15), (19) as before but with

$$\varphi_{r,s} := \frac{2 \Phi'(\varrho(f_{i,j}, v_{i,j}))}{v_{i,j}} \tag{21}$$

instead of (18). This equation system can again be solved by iterative linearisation.

4 Multi-Channel Images

Given a blurred multi-channel (such as RGB colour) image $\mathbf{f} = (f^c)_{c \in \Gamma}$ with the channel index set Γ , it is in most cases appropriate to assume equal blur in all channels, such that one seeks a multi-channel image \mathbf{u} and a single-channel PSF h that minimise

$$E(\mathbf{u}, h) = F(\mathbf{f}, \mathbf{u} * h) + \alpha R_u(\mathbf{u}) + \beta R_h(h), \tag{22}$$

where the single-channel data fidelity term (8) with ϱ from (6) or (9), and single-channel image regulariser $R_u(u) = \Psi(|\nabla u|^2)$ have been translated to the multi-channel setting as

$$F(\mathbf{f}, \mathbf{u} * h) = \Phi \left(\sum_{c \in \Gamma} \varrho(f^c, u^c * h) \right), \quad R_u(\mathbf{u}) = \Psi \left(\sum_{c \in \Gamma} |\nabla u^c|^2 \right). \tag{23}$$

By analogous derivations as in the previous sections, one obtains from (23) multi-channel minimisation methods that follow the general rule that nonlinearities are calculated by merging information from all channels, and are then applied uniformly in all channels, whereas the linear operations act separately in each channel.

Image estimation step. To apply this to the half-quadratic methods from [6, 14], notice first that they alternate between computing auxiliary quantities w_x, w_y by a (nonlinear) shrinkage step applied to image gradients, and updating the image u in a linear step via the Fourier domain. Consequently, w_x, w_y will turn into multi-channel counterparts computed by a joint multi-dimensional shrinkage operation, whereas the Fourier step is performed channelwise.

The multi-channel version of RRRL is found in [15]; in our setting it reads as

$$(u^c)^{k+1} = \frac{h^* * \left(\Phi'(\sum_d \varrho(f^d, v^d)) \frac{f^c}{v^c} \right) + \alpha [\operatorname{div}(\Psi'(\sum_d |\nabla u^d|^2) \nabla u^c)]_+}{h^* * \Phi'(\sum_d \varrho(f^d, v^d)) - \alpha [\operatorname{div}(\Psi'(\sum_d |\nabla u^d|^2) \nabla u^c)]_-} \tag{24}$$

where indices c and d refer to channels, and pixel indices i, j have been omitted.

PSF estimation step. In the estimation of h , operators C^v now map to a space of $|\Gamma|$ times as many dimensions than before but their convolution spectra remain to be of size $s_x s_y$, leaving the further computation of the Hessian (12) unchanged. In the equation systems of Section 3.2, the computation of the coefficients (16), (19) not involves a summation over channels, such as

$$S_{p,q;i,j} = \sum_{r,s} \sum_{c \in \Gamma} \varphi_{r,s}^c u_{r-i,s-j}^c u_{r-p,s-q}^c, \quad T_{p,q} = \sum_{r,s} \sum_{c \in \Gamma} \varphi_{r,s}^c f_{r,s}^c u_{r-p,s-q}^c. \quad (25)$$

The nonlinearities $\varphi_{r,s}$ require summation over channels in the argument of Φ , such that, for the symmetric penalisers, (18) becomes uniformly for all channels

$$\varphi_{r,s}^c \equiv \varphi_{r,s} = \Phi' \left(\sum_{d \in \Gamma} \varrho(f_{i,j}^d, v_{i,j}^d) \right), \quad \varrho \equiv \varrho_{\text{quad}} \text{ as in (6)}, \quad (26)$$

whereas, for the asymmetric penalisers, (21) turns into

$$\varphi_{r,s}^c = \frac{2 \Phi' \left(\sum_{d \in \Gamma} \varrho(f_{i,j}^d, v_{i,j}^d) \right)}{v_{i,j}^c}, \quad \varrho \equiv \varrho_{\text{RL}} \text{ as in (9)}. \quad (27)$$

5 Experiments

We begin by experiments on synthetic images, which allow a direct comparison of reconstructed images and PSFs with the ground truth, i.e. the original sharp image and the PSF used for its degradation. Unfortunately, quantitative measurements of PSNR or SSIM as are common for non-blind deconvolution evaluations face a difficulty in the case of blind deconvolution: As the convolution $u * h$ is invariant under opposite translations of u and h , reconstructions shifted by non-integer displacements must be treated as equally valid. In papers that do PSNR or SSIM measurements on blind deconvolution results, see [5, 13], some alignment between ground truth and reconstructed images is used to compensate for such shifts; however, no discussion is provided on how the interpolation involved in alignment influences the error measures. Preliminary tests indicate that already different direction of alignment (ground truth to reconstructed image, or vice versa?) can change PSNR by more than the PSNR differences reported for different methods. We believe therefore that further work is needed to put error measurements for blind deconvolution on more solid grounds. As we cannot solve this problem within the present contribution, we restrict ourselves to visual assessments here.

Figure 1(a) shows a test image from which a blurred version, Figure 1(b), was generated with the PSF shown in frame (g). Frames (c–f) show results of blind deconvolution with different method settings for the image and PSF estimation steps, with the corresponding reconstructed PSFs in (h–k). To ensure closeness of the results to the steady state, 300 iterations of the alternating minimisation were performed. The standard deviation in the LoG for computing the Hessian (12) was set to 2. Regularisation weights were $\alpha = 0.1$, $\beta = 10^6$ for frame (c), $\alpha = 0.003$, $\beta = 10^4$ for (d), $\alpha = 0.003$, $\beta = 10^4$ for (e), and $\alpha = 0.003$, $\beta = 3000$ for (f). The number of RRRL iterations in the image

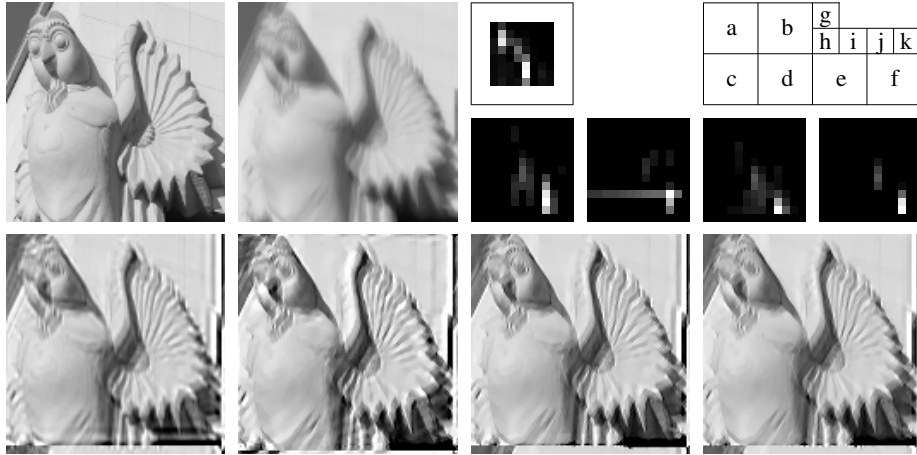


Fig. 1. (a) Test image, 128×128 pixels. (Clipped, downsampled and converted to greyscale from a photograph of the building of TU Vienna, Source of original image: https://upload.wikimedia.org/wikipedia/commons/e/e9/TU_Bibl_01_DSC1099w.jpg, Author: Peter Haas. Available under licence CC BY-SA 3.0.) – (b) Blurred by the PSF shown in frame (g). – (c) Deblurred using the method from [8]. – (d) Deblurred using the PSF estimation from [8] with image estimation by RRRL [16]. – (e) Deblurred using the robust PSF estimation from [9] with image estimation by RRRL. – (f) Deblurred using robust PSF estimation with asymmetric penalisation (8), (9). – (g) PSF (8×8 pixels) used to generate image (b), 2.85 times enlarged. – (h–k) PSFs (13×13 pixels each) reconstructed with the images (c–f), 2.85 times enlarged.

estimation of (d, e, f) was set to 300. In (e) and (f) 10 linearisation iterations were used in the PSF estimation step.

The sharpened images in Figure 1(c–f) demonstrate that the original method from [8], (c), as well as its robustified variants from [9], (e) and the present paper, (f), achieve reasonable sharpening, with a slight advantage for the robustified methods (e, f). The combination of robust image estimation with the non-robust PSF estimation from [8] as shown in frame (d) shows no clear advantage, which is no surprise as the combination of a non-robust and robust data fidelity term is even a more blatant mismatch than that of two robust data terms in frame (e). Among the two robust methods (e), (f) there is no clear visual preference. The reconstructed PSFs (h–k) complement these findings. The robust methods yield visually the best matches (j, k) to the ground truth (g). The method from [8] yields an acceptable estimate (h), whereas the estimate (i) from the half-robust approach appears to be the farthest off.

In Figure 2(a), the blurred image from Figure 1(b) was further degraded by Gaussian noise. For this image, a non-blind RRRL deconvolution result ($\alpha = 0.01$, 300 iterations) using the ground-truth PSF is shown in Figure 2(b). Frames (c–f, h–k) show blind deconvolution results with the same methods as in Figure 1. Here, 300 iterations of the alternating minimisation were used (no visible changes after about 150 iterations). The standard deviation in the LoG was increased to 5 for frames (c, d, e). Regularisation

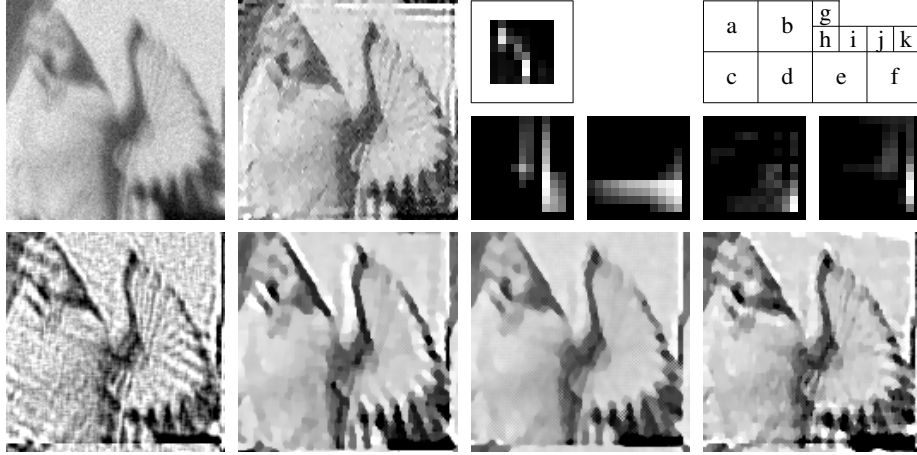


Fig. 2. (a) Blurred test image from Fig. 1(b) degraded by Gaussian noise with standard deviation 10. – (b) Non-blind RRRL deconvolution of (a) using PSF (g). – (c) Blind deconvolution using the method from [8]. – (d) Deblurred using the PSF estimation from [8] with image estimation by RRRL [16]. – (e) Deblurred using the robust PSF estimation from [9] with image estimation by RRRL. – (f) Deblurred using robust PSF estimation with asymmetric penalisation (8), (9). – (g) PSF (8×8 pixels) used to generate image (a), 2.85 times enlarged (same as Fig. 1(g)). – (h–k) PSFs (13×13 pixels each) reconstructed with the images (c–f), 2.85 times enlarged.

weights were $\alpha = 0.1$, $\beta = 3 \cdot 10^7$ in (c), $\alpha = 0.01$, $\beta = 10^8$ in (d), $\alpha = 0.02$, $\beta = 10^5$ in (e), $\alpha = 0.01$, $\beta = 10^6$ in (f). The remaining parameters were chosen as in Figure 1.

As can be expected, the added noise in the input image reduces the quality of deconvolution results significantly. However, it is evident that particularly the results of the fully robust methods (e, f) suffer from less ringing artifacts and noise amplification than the non-robust result (c). Among the reconstructed PSFs (h–k) the one obtained by our proposed method (k) is visually the best match to the ground truth (g).

As a real-world example, Figure 3 presents tests on two RGB images (a, e) blurred during acquisition. The PSF estimation from [8], [9] and our method (8), (9) are juxtaposed, using RRRL with $\alpha = 0.002$ and 300 iterations for image estimation in all cases. 500 iterations of the alternating minimisation were used. The PSF regularisation weight β was set to 10^5 for [8], 300 for [9] and 1000 for our method. For the robust methods, three linearisation iterations were used. Both robust methods yield some improvement over [8]. From the second test image (e), some details seem to have been recovered sharper by our method (h) than by the one from [9], see (g), whereas for the first test image (a) the quality of both robust methods (c, d) is about the same.

6 Summary and Outlook

Based on the robust blind deconvolution approach from [9], we have presented an improved model that uses the same data fidelity term for image and PSF estimation. Our model represents a consistent minimisation procedure for a joint energy functional

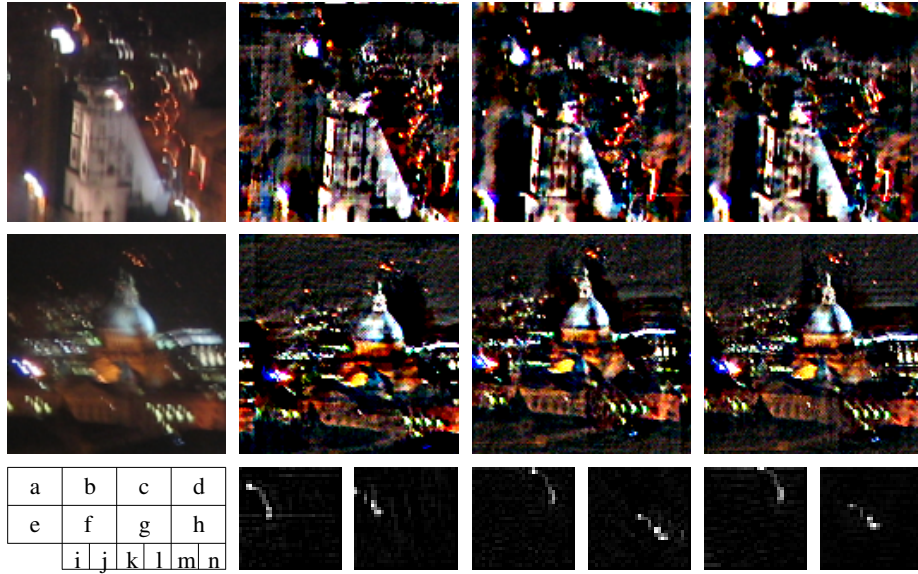


Fig. 3. (a, e) Blurred photographs, 128×128 pixels each (Author: Gregor Peltri). – (b, f) Deblurred using the PSF estimation from [8] and RRRL for image estimation. – (c, g) Deblurred using the robust PSF estimation from [9] and RRRL. – (d, h) Deblurred using the robust PSF estimation (8), (9) and RRRL. – (i–n) PSFs (31×31 pixels each, 1.93 times enlarged) for (b, f, c, g, d, h), respectively.

which opens up the way for more detailed theoretical analysis in the future. We have shown by experiments the viability of our method for synthetic and real-world examples, and the advantage of the robust approaches from [9] and the present paper over their non-robust predecessor from [8] in deblurring input images with moderate noise.

From the two conflicting data fidelity terms in [9] we have favoured here the asymmetric one that is related to Poisson-type noise. It remains a desiderate to come up with a similar consistent model using symmetric robust data fidelity terms. This will require further work on minimisation procedures, as the half-quadratic approach from [6, 14] underlying the image estimation in [8] is difficult to adapt to a robust setting.

Whereas for most parameters of the method heuristics yield good results, see the settings used in Section 5, further analysis of parameter selection, especially for the regularisation weights, remains a topic of future work. The high computational cost that is typical for blind deconvolution renders further effort on algorithmic optimisations worthwhile. As pointed out in Section 5, future work is also needed regarding appropriate quantitative measures for blind deconvolution.

References

1. Bar, L., Sochen, N., Kiryati, N.: Image deblurring in the presence of salt-and-pepper noise. In Kimmel, R., Sochen, N., Weickert, J., eds.: Scale Space and PDE Methods in Computer

- Vision. Volume 3459 of Lecture Notes in Computer Science. Springer, Berlin (2005) 107–118
2. Chan, T.F., Wong, C.K.: Total variation blind deconvolution. *IEEE Transactions on Image Processing* **7** (1998) 370–375
 3. Elhayek, A., Welk, M., Weickert, J.: Simultaneous interpolation and deconvolution model for the 3-D reconstruction of cell images. In Mester, R., Felsberg, M., eds.: *Pattern Recognition*. Volume 6835 of Lecture Notes in Computer Science. Springer, Berlin (2011) 316–325
 4. Huber, P.J.: *Robust Statistics*. Wiley, New York (1981)
 5. Köhler, R., Hirsch, M., Mohler, B., Schölkopf, B., Harmeling, S.: Recording and playback of camera shake: Benchmarking blind deconvolution with a real-world database. In Fitzgibbon, A., Lazebnik, S., Perona, P., Sato, Y., Schmid, C., eds.: *Computer Vision – ECCV 2012, Part VII*. Volume 7578 of Lecture Notes in Computer Science. Springer, Berlin (2012) 27–40
 6. Krishnan, D., Fergus, R.: Fast image deconvolution using hyper-Laplacian priors. In: *Advances in Neural Information Processing Systems*. (2009) 1033–1041
 7. Levin, A., Weiss, Y., Durand, F., Freeman, W.T.: Efficient marginal likelihood optimization in blind deconvolution. In: *IEEE Conference on Computer Vision and Pattern Recognition*. (2011) 2657–2664
 8. Liu, G., Chang, S., Ma, Y.: Blind image deblurring using spectral properties of convolution operators. *IEEE Transactions on Image Processing* **23** (2014) 5047–5056
 9. Moser, P., Welk, M.: Robust blind deconvolution using convolution spectra of images. In Niel, K., Roth, P.M., Vincze, M., eds.: *1st OAGM-ARW Joint Workshop: Vision Meets Robotics, Wels, Austria, Österreichische Computer-Gesellschaft* (2016) 69–78
 10. Perona, P., Malik, J.: Scale space and edge detection using anisotropic diffusion. *IEEE Transactions on Pattern Analysis and Machine Intelligence* **12** (1990) 629–639
 11. Persch, N., Elhayek, A., Welk, M., Bruhn, A., Grewenig, S., Böse, K., Kraegeloh, A., Weickert, J.: Enhancing 3-D cell structures in confocal and STED microscopy: a joint model for interpolation, deblurring and anisotropic smoothing. *Measurement Science and Technology* **24** (2013) 125703
 12. Rudin, L.I., Osher, S., Fatemi, E.: Nonlinear total variation based noise removal algorithms. *Physica D* **60** (1992) 259–268
 13. Schelten, K., Nowozin, S., Jancsary, J., Rother, C., Roth, S.: Interleaved regression tree field cascades for blind image deconvolution. In: *IEEE Winter Conference on Applications of Computer Vision*. (2015) 494–501
 14. Wang, Y., Yang, J., Yin, W., Zhang, Y.: A new alternating minimization algorithm for total variation image reconstruction. *SIAM Journal on Imaging Sciences* **1** (2008) 248–272
 15. Welk, M.: A robust variational model for positive image deconvolution. Technical Report cs:1310.2085, arXiv.org (2013)
 16. Welk, M.: A robust variational model for positive image deconvolution. *Signal, Image and Video Processing* **10** (2016) 369–378
 17. Welk, M., Raudaschl, P., Schwarzbauer, T., Erler, M., Läter, M.: Fast and robust linear motion deblurring. *Signal, Image and Video Processing* **9** (2015) 1221–1234
 18. Welk, M., Theis, D., Weickert, J.: Variational deblurring of images with uncertain and spatially variant blurs. In Kropatsch, W., Sablatnig, R., Hanbury, A., eds.: *Pattern Recognition*. Volume 3663 of Lecture Notes in Computer Science. Springer, Berlin (2005) 485–492
 19. Xu, L., Jia, J.: Two-phase kernel estimation for robust motion deblurring. In Daniilidis, K., Maragos, P., Paragios, N., eds.: *Computer Vision – ECCV 2010, Part I*. Volume 6311 of Lecture Notes in Computer Science. Springer, Berlin (2010) 157–170
 20. You, Y.L., Kaveh, M.: Anisotropic blind image restoration. In: *Proc. 1996 IEEE International Conference on Image Processing*. Volume 2., Lausanne, Switzerland (1996) 461–464
 21. Zervakis, M.E., Katsaggelos, A.K., Kwon, T.M.: A class of robust entropic functionals for image restoration. *IEEE Transactions on Image Processing* **4** (1995) 752–773